The role of platform margin collapses and slope landslides in the initiation and evolution of submarine canyons

Junjin Chen[1,2,3,4], Qi Li[1,3,4*], Shiguo Wu[2*] and Shiqiao Liu[5]

[1]School of Ocean Sciences, China University of Geosciences, Beijing, China, [2]Institute of Deep-Sea Science and Engineering, Chinese Academy of Sciences, Sanya, China, [3]Hainan Institute of China University of Geosciences (Beijing), Sanya, China, [4]Key Laboratory of Polar Geology and Marine Mineral Resources (China University of Geosciences, Beijing), Ministry of Education, Beijing, China, [5]Haikou Marine Geology Survey Center, China Geology Survey, Haikou, China

The Zhongsha Platform is the largest modern isolated carbonate platform of around 8600 km^2 in the South China Sea, providing a unique case study for sedimentary processes in pure carbonate settings. High-resolution multibeam bathymetric data, two-dimensional seismic profiles, and surface sediment cores are utilizes to reveal the initiation and evolution of submarine canyons on the northeastern slope of the Zhongsha Platform. Three submarine canyons are revealed within the survey area that incise the slope at water depths between 600 and 4100 m. C1 presents a linear pattern, whereas C2 and C3 exhibit dendritic morphologies. A large-scale scalloped collapse has deeply excavated the platform margin and slope. Within this catastrophic failure, C2 originated in a northeastward orientation and subsequently converted to an eastward direction with a length of 54.8 km. It is distinguished by the erosion of numerous tributaries in the upper course, the transition of flow direction in the middle course, and the presence of retrogressive landslides in the lower course. Slope landslides extend eastward from middle-lower slope towards the oceanic basin at water depths ranging from 2300 to 4200 m. A series of scarps and immature canyons have developed with escarpments showing pronounced relief at the landslide heads. The triggering mechanisms of platform margin collapses and slope landslides are attributed to sediment aggradation, slope oversteepening, gravity flows, relative sea-level changes, surface monsoon currents, and deep cyclonic circulation. The canyon evolution is explained through four stages: Inception stage, sediment instability on platform margin and slope-toe; Expansion stage, the presence of platform margin collapses and slope landslides; Development stage, the initiation of submarine canyons eroded by gravity flows with downslope and retrogressive erosion; Present stage, the upper slope canyon incised into the landslide area and ultimately integrated with the lower slope canyon, creating an elongated modern canyon. This work contributes to enhance our understanding of the detailed morphology, transport processes, and triggering mechanisms of submarine canyons in the pure carbonate systems.

1 Introduction

Submarine canyons, with linear or meandering paths, are key conduits that incise across continental/platform slopes extending into deep-water environments (Shepard, 1972; Posamentier, 2003; Mulder et al., 2012; Li et al., 2023). Recent research has highlighted the crucial role of submarine canyons in delivering significant quantities of sediments, pollutants, and nutrients from shallow to deep-sea settings (Tubau et al., 2015; Zhong and Peng, 2021; Heijnen et al., 2022), sculpting submarine geomorphology (Almeida et al., 2015; Ribeiro et al., 2021; Sun et al., 2023), preserving sedimentary and climatic records for reconstructing paleoenvironment (Principaud et al., 2017; Wunsch et al., 2018; Su et al., 2020), and being recognized as important hydrocarbon reservoirs (Mayall et al., 2006; Janocko et al., 2013; Li et al., 2020).

In isolated carbonate platform systems, the absence of terrigenous materials is the precondition for the development of pure carbonate environments (Wu et al., 2014; Reijmer, 2021). The uplifted platforms serve as catchment areas where carbonate sediments are produced, accumulated, and preserved (Jorry et al., 2016; Counts et al., 2018). Carbonate-producing organisms, such as coral reefs, calcareous algae, and mollusks, are the primary source of carbonate sediments growing on the platform top (Pomar and Hallock, 2008; Betzler et al., 2021). The carbonate production is strongly influenced by temperature, light, salinity, nutrients, sea-level changes, and hydrodynamic conditions at a local scale (Lees, 1975; Pomar, 2001; Schlager, 2005). During sea-level highstands, the increased water depth allows for higher carbonate production, leading to the accumulation of substantial amounts of sediments on the platform top (Wilson and Roberts, 1992; Schlager et al., 1994). Subsequently, off-platform sediment transport can be initiated and enhanced by waves, tidal currents, and surface ocean circulation (Wilson and Roberts, 1995; Betzler et al., 2014). Transport processes from platform-top to adjacent slopes can trigger large-scale gravitational collapses along the platform margin, initiate turbidity currents capable of incising submarine canyons, and lead to slope instabilities that can activate submarine landslides (Tournadour et al., 2017; Etienne et al., 2021; Chen et al., 2022; Petrovic et al., 2023). These mass wasting processes exert pivotal function in facilitating the export of platform-derived sediments into deep-water environments and sculpting the morphology of platform margin and slope.

The formation of submarine canyons can be attributed to various factors, such as downslope erosive gravity flows, retrogressive slope landslides, earthquakes, and tectonic events (Harris and Whiteway, 2011; Courgeon et al., 2016; Mountjoy et al., 2018; Wu et al., 2022). Tectonic uplift can lead to relative sea-level changes and create pathways that facilitate the movement of gravity-driven sediment flows (Serra et al., 2020; Wang et al., 2023). The development and evolution of submarine canyons are subject to sediment supply, downslope erosional processes, ocean currents, and the surrounding seafloor topography, which interact together to shape the diversity of canyon morphology (Saller and Dharmasamadhi, 2012; Liu et al., 2016; Yu et al., 2021; Warnke et al., 2023). Most previous research on these triggering mechanisms of canyons have focus on siliciclastic depositional systems, whereas relatively little work exists on the modern submarine canyons in isolated carbonate platform settings (McHargue et al., 2011; Tournadour et al., 2017; Lemay et al., 2020; Pettinga and Jobe, 2020). Carbonate sediments are influenced by carbonate production and reef development, and sea-level highstands contribute to higher carbonate production and off-platform transport (Wilson and Roberts, 1995; Schlager, 2005; Jorry et al., 2016). In contrast, siliciclastic sediments are controlled by terrestrial sources, and sea-level lowstands contribute to seaward erosion and progradation (Haq et al., 1987; Koss et al., 1994). Although recent studies have expanded into modern carbonate factories around the world, such as the Bahama Banks (southeast Florida), Lansdowne Bank (Southwest Pacific Ocean), Maldives (Indian Ocean), and Great Barrier Reef (northeast Australia), with an area of 18000, 4000, 298, and 348700 km^2, respectively (Puga-Bernabéu et al., 2011, 2013; Betzler et al., 2015; Mulder et al., 2017; Reolid et al., 2020; Etienne et al., 2021; Fauquembergue et al., 2023), the complexity and multiplicity of canyon origins and mechanisms on the platform slopes receive less documentation and need further exploration. The Zhongsha Platform, acclaimed as one of the world's largest isolated carbonate platforms with an area of 8600 km^2, offers a unique case study in pure carbonate settings and significantly enhances the global understanding of sedimentary processes along carbonate slopes.

In this study, the geomorphology, formation, and evolution of submarine canyons on the northeastern slope of the Zhongsha Platform are investigated based on multibeam bathymetric, two-dimensional seismic, and sediment grain size data. The specific objectives are to 1) quantitatively analyze the key geomorphic characteristics of submarine canyons and slope landslides, 2) discuss the triggering mechanisms in initiating submarine canyons, and 3) establish an evolution model of submarine canyons in the pure carbonate systems.

2 Geological background

The South China Sea (SCS) is the largest marginal sea in the northwestern Pacific Ocean (Figure 1). It originated from episodes of continental rifting and subsequent seafloor spreading that occurred from the Late Cretaceous to the Early Miocene, followed by post-spreading thermal subsidence from the Middle Miocene to the present (Taylor and Hayes, 1983; Franke et al., 2014; Li et al., 2014). Large canyon systems developing along the northern margin of the SCS include the Pearl River Canyon, Central Canyon, and Taixinan Canyon, which extend from the continental shelf to the abyssal plain (Figure 1; Su et al., 2020). Tropical carbonate platforms have thrived on the uplifted basement and volcanic structures since the Early Oligocene, with particular emphasis on the Zhongsha, Dongsha, Xisha, and Nansha islands (Yao et al., 2012; Wu et al., 2016). The Zhongsha Platform, situated in the transition zone between the northern continental slope and central basin, is the largest modern isolated carbonate platform in the SCS (Figure 1). It exhibits a NE-SW orientation with a water depth ranging from 17 to 600 m. Numerous submarine canyons and
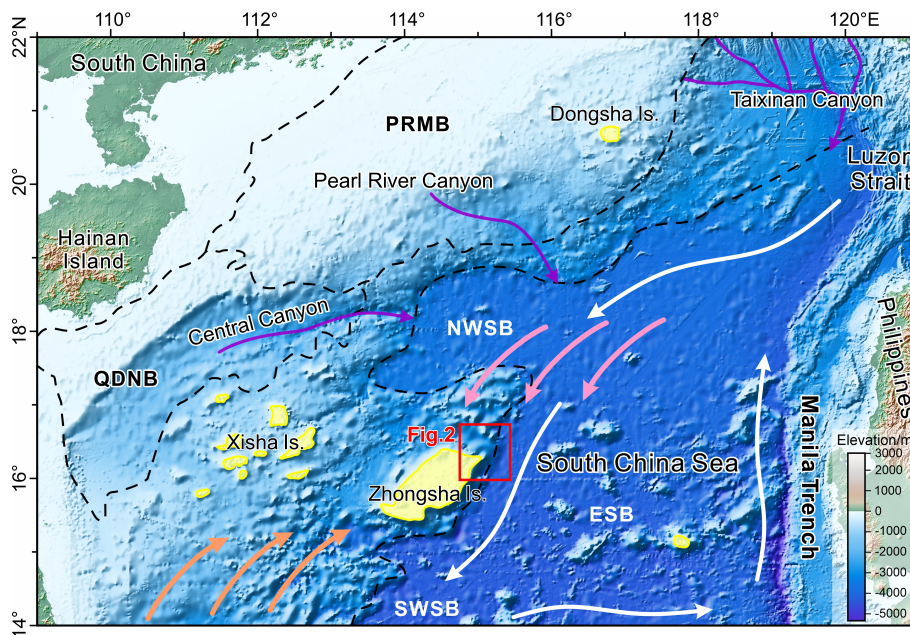
FIGURE 1
Topographic map of the South China Sea showing the location of the study area. Purple arrows represent the main canyon systems (Su et al., 2020). Pink and orange arrows represent the monsoon currents during winter and summer, respectively (Fang et al., 2012). White arrows indicate the deep cyclonic circulation pattern in the oceanic basin (Wang et al., 2018). Yellow patches mark the modern reefs and islands (Wu et al., 2016). Black dashed lines delineate the basin boundaries. QDNB, Qiongdongnan Basin; PRMB, Pearl River Mouth Basin; ESB, East Sub-basin; NWSB, Northwest Sub-basin; SWSB, Southwest Sub-basin.

landslides are developed along the entire margin and slope of the Zhongsha Platform (Chen et al., 2024).

The Luzon Strait, with a maximum sill depth of about 2,400 m, is the only deep connection between the SCS and the Pacific Ocean (Figure 1; Yang et al., 2002; Qu et al., 2006). The strong diapycnal mixing in the deep SCS drives a persistent pressure gradient, which in turn leads to deepwater overflow from the Pacific into the SCS (Yang et al., 2016; Xu et al., 2023). The ocean circulation in the SCS exhibits a vertically three-dimensional structure, comprising surface, middle, and deep currents that follow cyclonic, anticyclonic, and cyclonic patterns, respectively. This circulation pattern is mainly affected by the Southeast Asian monsoon with seasonal variations, the intrusion of the Kuroshio current, and the overflow of deepwater through the Luzon Strait (Zhu et al., 2019; Gan et al., 2022; Shen et al., 2022).

3 Data and methods

3.1 Bathymetric data

The multibeam bathymetric data covered the northeastern Zhongsha Platform, extending from platform top to oceanic basin, with a spatial resolution of 100 m (Figure 2A). This data was performed by KONGSBERG EM302 system, processed using CARIS HIPS and SIPS software, and analyzed with Global Mapper software. The high-resolution multibeam bathymetric data provided ample details to detect and depict submarine canyons, slope landslides and other sedimentary features around the

Zhongsha Platform at water depths ranging from 100 to 4200 m. The morphometric parameters of submarine canyons were measured, including depth, length, width, slope gradient, elevation difference, and sinuosity. Similarly, the morphometric parameters were calculated for slope landslides, encompassing depth, length, width, elevation difference, and area.

3.2 Seismic data

The two-dimensional multi-channel seismic data provided good images across the northeastern Zhongsha Platform and were utilized to identify the seismic reflection characteristics of various depositional features (Figure 2A). The seismic source was GI gun with a total volume of 540 in^3, towed at a water depth of 5 m. The streamer was 500 m long with a trace spacing of 6.25 m. The sampling frequency was 1.0 ms and the record length was 8 s. The seismic data were processed using PARADIGM 2017 system and interpreted with GeoEast software. The total length of seismic data used in this study is about 172 km, with a resolution of 20 m. The seismic interpretation (e.g., seismic facies analysis) is based on the seismic and depositional features.

3.3 Sediment samples

Six sediment samples were collected from the seafloor surface using box samplers with a length of 25 cm. Core BC1 was collected from the platform top, BC2 from the middle course of C2, BC3 from
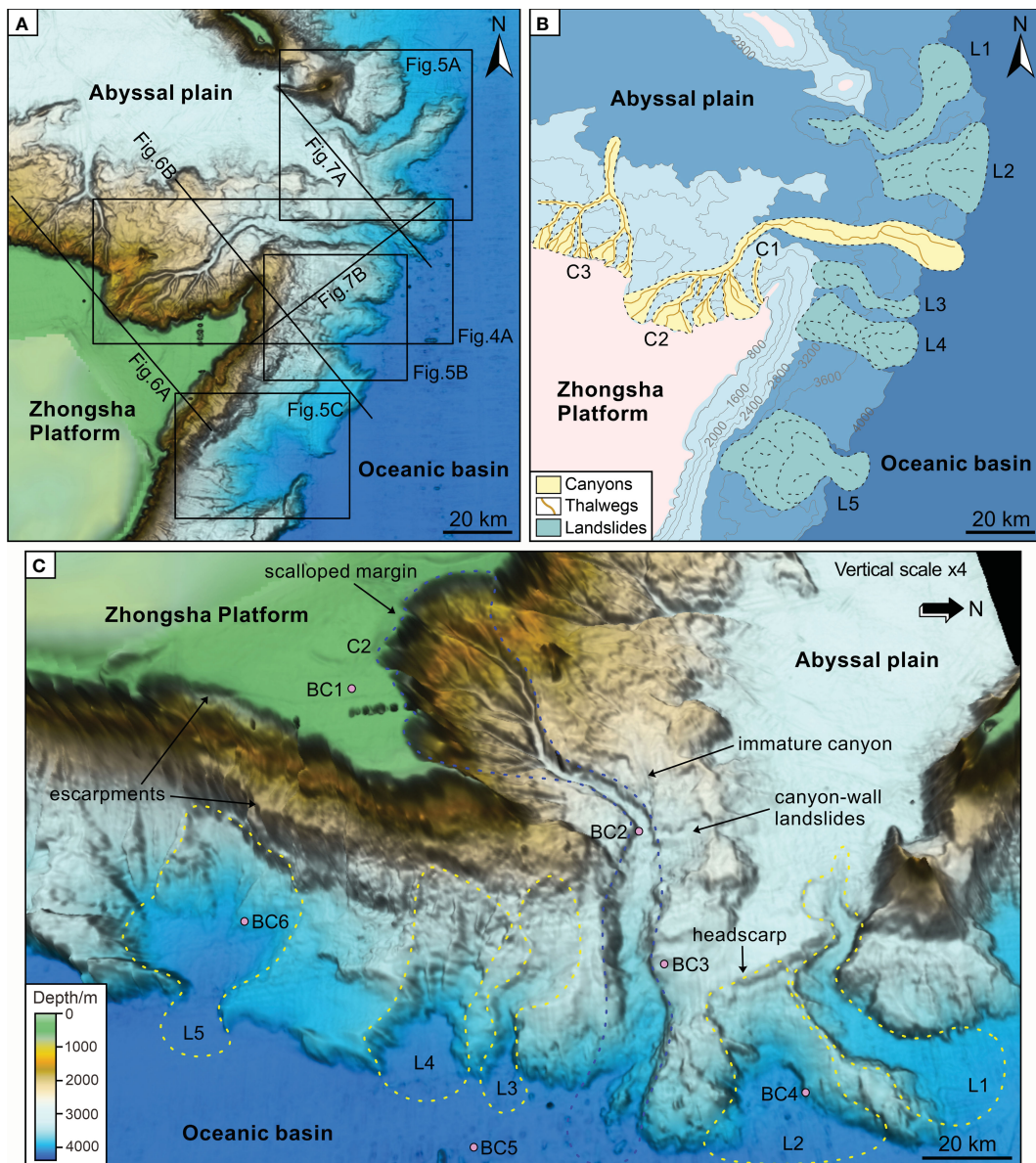
FIGURE 2
(A) Multibeam bathymetric map showing detailed seafloor morphology in the northeast Zhongsha Platform. Black lines indicate the location of seismic profiles. **(B)** Sketch map highlighting the submarine canyons (C1-C3) and landslides (L1-L5) in the study area. **(C)** Three-dimensional topographic view emphasizing carbonate platform, canyons, and landslides. Purple circles indicate the positions of surface sediment cores (BC1-BC6).

the sidewall of C2, BC4 from the L2, BC5 from the oceanic basin, and BC6 from the L5 (Figure 2C). These surface samples are mainly composed of silt and clay, without gravel content. Grain size measurements were conducted using Beckman Coulter LS13 320 laser diffraction particle size analyzer, with a measuring range of 0.01-2000 µm and a repeatability error of 0.5%. Each sample was tested three times, and the average value of the test results was calculated. The Udden–Wentworth standard was employed for grain size classification (Wentworth, 1922). The components of clay, silt, and sand correspond to sediments with grain sizes of <4 µm, 4-63 µm, 63-2000 µm, respectively.

4 Results

4.1 Morphology of submarine canyons

The margin of the Zhongsha Platform is demarcated by the 500-600 m isobath (Figure 2A). The slope gradient spans from 4.6 to 48.6° in the north and ranges between 5.1 and 59.1° in the east, with the steepest gradients occurring at the escarpments along the platform margin (Figures 3B, D, F). Three submarine canyons, identified as C1, C2, and C3 from east to west, are observed on the northeastern slope of the Zhongsha Platform (Figures 2A, B). C1
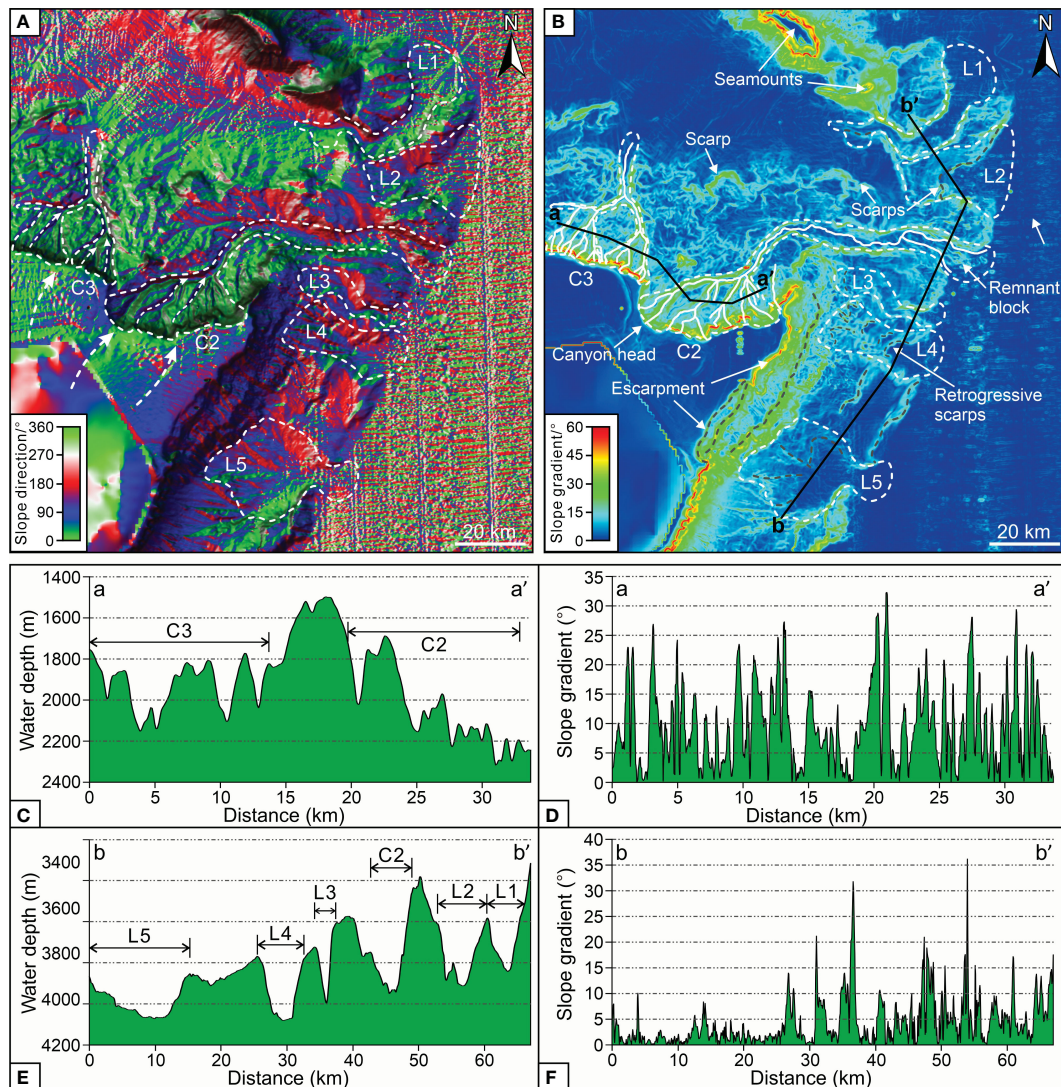
FIGURE 3
(A) Slope direction map (aspect map) highlighting the downslope trending linear and massive depressions in the study area. (B) Slope gradient map emphasizing the gradient relief of seafloor topography. (C, D) Bathymetric and slope gradient profiles across the northern slope of the Zhongsha Platform showing the geometry of submarine canyons. (E, F) Bathymetric and slope gradient profiles across the eastern slope of the Zhongsha Platform displaying the geometry of slope landslides.

shows a linear morphology, while C2 and C3 exhibit dendritic patterns. The morphometric values of canyons are provided in Table 1. The continuous and linear depressions are identified along the platform slope highlighting the paths of canyons (Figure 3A). They extend from platform top to peripheral slopes and ultimately reach the deep-sea regions. The canyons exhibit steep-sided V-shaped profiles in the upper course and U-shaped profiles in the lower course (Figures 3C, E). C1, the shortest canyon without tributaries, reaches its terminus on the middle slope at a water depth of 2602 m, with a length of 6.98 km and a sinuosity of 1.05 (Figure 2B). C2, the longest, widest, and deepest canyon with numerous tributaries, spans water depths ranging from 651 to 4115 m, with a length of 54.8 km, an average thalweg gradient of 4.5° and a sinuosity of 1.24 (Figures 2B, C). C3, with a length of 21.25 km and a sinuosity of 1.13, initiates at a water depth of 577 m with numerous tributaries and terminates at a water depth of

4080 m (Figure 2B). C2 exhibits a significant elevation difference and directly connects with the oceanic basin to the east, while C3 comes to an end at the abyssal plain to the north.

A large-scale scalloped margin, with a perimeter measuring about 36 km, has developed on the northeast Zhongsha Platform, representing the canyon head of C2 (Figures 2A, 4A). C2 is initially oriented in a northeastward direction and subsequently undergoes a directional transition towards the east at a water depth of approximately 3050 m. In the upper course of C2, three main sub-canyons (C2a, C2b, and C2c) converge into the C2 at water depths of 2450, 2650, and 2700 m, respectively (Figures 4A, B). Within the lower course of C2, eight knickpoints (K1-K8) are discovered and present significant changes in slope gradient, with an average slope of 6° (Figures 4A, B). The lower knickpoints are more mature than the upper knickpoints. The two tributaries at the end of C2 are separated by remnant blocks (Figure 4A). C2 progressively widens as it descends

TABLE 1   Summary of morphometric parameters of submarine canyons.

Submarine canyon	Depth (m)		Length (km)	Avg. width (m)	Avg. gradient (°)	Elevation difference (m)	Sinuosity
	Min	Max					
C1	741	2602	6.98	652	15.7	1861	1.05
C2	651	4115	54.80	3050	4.5	3464	1.24
C2a	623	2455	10.51	1906	11.9	1832	1.20
C2b	604	2652	8.31	1061	12.5	2048	1.13
C2c	638	2697	8.88	1049	14.3	2059	1.10
C3	577	2970	21.25	1105	7.2	2391	1.13

downslope, with an average slope gradient of 5.08° in the upper course and 2.45° in the lower course (Figures 4B, C). The cross-section profiles of C2 feature roughly symmetrical canyon walls, presenting V-shaped in the upper course and evolving to U-shaped in the lower course (Figure 4C). C1 could erode downslope and then converge with C2, serving as a tributary canyon.

4.2 Morphology of slope landslides

Five slope landslides, designated as L1 to L5 from north to south, are observed on the northeast Zhongsha Platform adjacent to the oceanic basin (Figures 2B, C). The morphometric parameters of landslides are attached in Table 2. The continuous and massive depressions are perceived along the platform slope revealing the traces of landslides (Figure 3A). They prolong from middle-lower slope towards oceanic basin trending in an eastward direction. The landslides present elongated shape in the plane view and concave shape in the cross-section profile, with notable slope gradients along their headwalls and lateral margins (Figures 3, 5). L1, the longest landslide with immature canyon morphology, is distributed from abyssal plain to oceanic basin, with a water depth of 2810-4041 m, a length of 33.8 km, an average width of 4.4 km, and an area of 133.1 km^2 (Figures 5A, D). The linear retrogressive erosion is observed on the head of L1. L2, the shortest landslide with smallest elevation difference of 928 m, is excavated in the north of the lower course of C2, with a water depth of 3220-4148 m, a length of 15.6 km, an average width of 8.3 km, and an area of 133.1 km^2 (Figures 5A, D). L3 is distinguished as
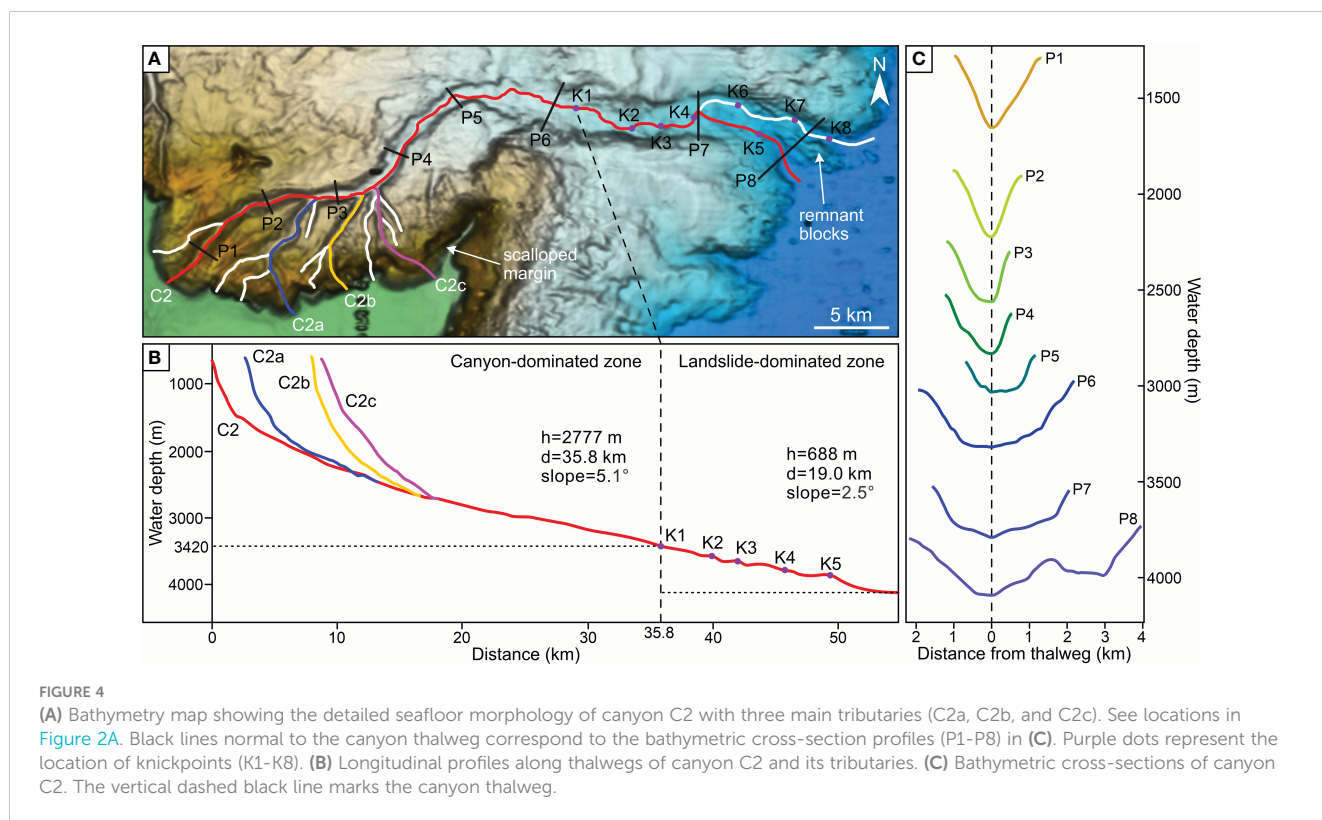
FIGURE 4
(A) Bathymetry map showing the detailed seafloor morphology of canyon C2 with three main tributaries (C2a, C2b, and C2c). See locations in Figure 2A. Black lines normal to the canyon thalweg correspond to the bathymetric cross-section profiles (P1-P8) in (C). Purple dots represent the location of knickpoints (K1-K8). (B) Longitudinal profiles along thalwegs of canyon C2 and its tributaries. (C) Bathymetric cross-sections of canyon C2. The vertical dashed black line marks the canyon thalweg.

TABLE 2 Summary of morphometric parameters of submarine landslides.

Submarine landslide	Depth (m)		Length (km)	Avg. width (km)	Elevation difference (m)	Area (km²)
	Min	Max				
L1	2810	4041	33.8	4.4	1231	133.1
L2	3220	4148	15.6	8.3	928	133.4
L3	2309	4160	21.7	3.4	1851	67.9
L4	2732	4185	21.1	6.9	1453	142.1
L5	2823	4192	23.6	9.4	1369	192.7

the narrowest and smallest landslide with biggest elevation difference of 1851 m, featuring an immature canyon morphology and covering an area of 67.9 km². It is observed in the south of the lower course of C2, with a water depth of 2309-4160 m, a length of 21.7 km, and an average width of 3.4 km (Figures 5B, D). L4 is preserved on the northeastern platform slope, characterized by a water depth between 2732 and 4185 m, a length of 21.1 km, an average width of 6.9 km, and an area of 142.1 km² (Figures 5B, D). L5, the largest and widest landslide with remarkable escarpments located on the eastern platform slope, extends across a water depth from 2823 to 4192 m, with a length of 23.6 km, an average width of 9.4 km, and an area of 192.7 km² (Figures 5C, D). L1 and L3 present slightly concave shape along their longitudinal bathymetry profile, whereas L2, L4, and L5 display highly concave morphology (Figure 5D). A series of scarps and immature canyons have developed within the landslides, and cyclic escarpments exhibit pronounced relief at the head of landslides (Figures 2C, 5).

4.3 Seismic facies characteristics

Seismic facies characteristics are summarized in Table 3. The uplifted carbonate platform, composed of authigenic carbonate rocks (Jorry et al., 2020), is characterized by discontinuous, high amplitude, and internal chaotic reflection, with convex-up mound shape (Figure 6A). The inner-platform lagoon deposits exhibit continuous to simi-continuous, low to moderate amplitude seismic features with vertical accretion (Figure 6A). A series of reefs have accumulated vertically on the platform margin, characterized by a positive topographic relief with a simi-continuous, high amplitude, and internal chaotic reflection, contributing to the formation of a rimmed platform margin (Figure 6A). Gravity flow deposits have extensively propagated across the platform top, overlaying the inner-platform deposits and tilting towards the canyons and escarpments. These deposits are marked by horizontal, continuous, moderate to high amplitude seismic reflections (Figure 6A). Mass transport deposits, distinguished by headscarps, lateral margins, and inner scarps, are widely distributed across the platform slopes and within the canyon floors. They exhibit discontinuous, low to high amplitude, chaotic or semi-transparent acoustic facies (Figures 6, 7). Large-scale slope landslides have developed along the entire right side of C2, delivering sediments from slope into canyon with a maximum transport distance of 7.2 km (Figures 2A, 6B). Submarine canyons exhibit continuous and high amplitude seismic reflections, confined within a V- or U-shaped

erosional surface (Figures 6, 7). In the lower course of C2, the slope deposits are characterized by cyclic steps, with simi-continuous and low to high amplitude seismic reflections, which are most likely initiated by overspilled turbidity currents (Figures 7B, D). Several significant escarpments are discovered along the eastern platform slope at the head regions of L3, L4, and L5 (Figures 6B, 7B). Canyon features, such as immature canyon and canyon migration, are developed within the slope landslides (Figure 6B). The pelagic deposits in the abyssal plain are characterized by parallel, continues, and low to high amplitude seismic reflections (Figures 6B, 7A).

4.4 Surface sediment features

Grain size analysis of surface sediments reveals a marked dominance of sand in BC1, up to about 84%, and silt in BC2-BC6, ranging from 56 to 65% (Figure 8, Table 4). Relatively coarser grain sizes (>250 µm, medium sand) are only found on the platform top, whereas relatively finer grain sizes (<4 µm, clay) mostly occur io the lower platform slope and deep-sea basin. The cumulative curve of BC1 presents highly convex with a steep gradient, while those of BC2 to BC6 present a similar sinuous trend with gentle gradients (Figure 8A). The frequency curves, with the volume percentage less than 5%, exhibit a single peak in BC1, three peaks in BC2, BC3, and BC4, and four peaks in both BC5 and BC6 (Figure 8B). The main peak of BC1 is distributed in middle sand with a sharp shape and a grain size of 340 µm (Figure 8B). The primary peak of BC2 is associated with fine silt with a grain size of 6 µm, while the second and third peaks are distributed in coarse silt and fine clay with grain sizes of 6 and 0.8 µm, respectively (Figure 8B). In BC3, the top peak corresponds to fine silt with a grain size of 7.4 µm, the secondary peak is attributed to fine clay with a grain size of 0.9, and the third peak is distributed in fine sand with a grain size of 92 µm (Figure 8B). The main peak of BC4 almost overlaps with that of BC3, and the graine size of third peak in BC4 is consistent with that observed in BC2. The second peak of BC4 is distributed in fine sand with a grain size of 122 µm. BC5 and BC6 demonstrate analogous curves with four distinct peaks corresponding to fine sand, coarse silt, fine silt, and fine clay from high to low frequency (Figure 8B). In general, the trends of grain size distribution from BC2 to BC6 is relatively analogous, while BC1 demonstrates a completely different pattern from them.
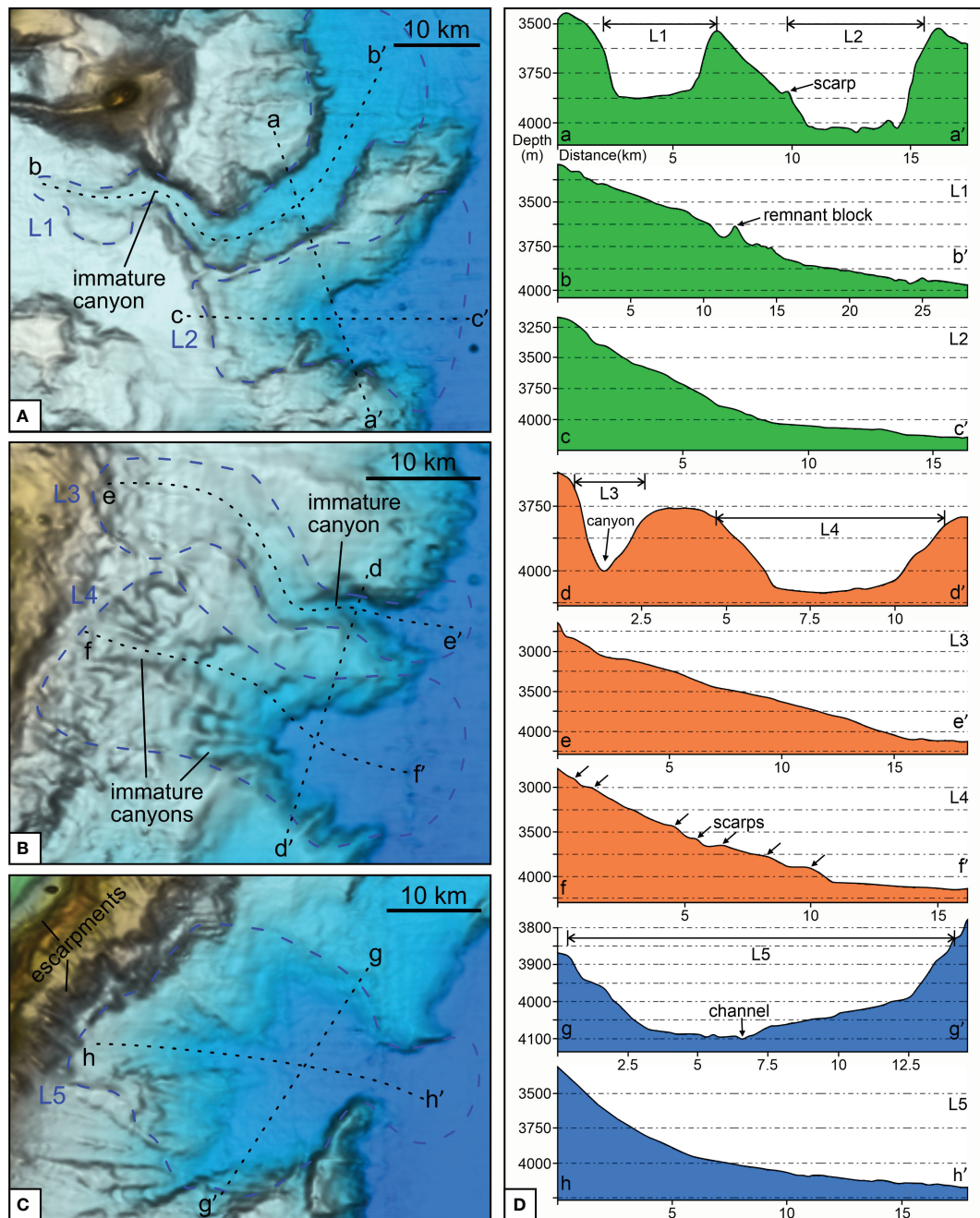
FIGURE 5
(A–C) Bathymetry map showing the detailed seafloor morphology of slope landslides (L1 to L5). See locations in Figure 2A. Blue dashed lines indicate the boundaries of slope landslides. Black dashed lines correspond to the bathymetry profiles in (D). (D) Bathymetry profiles showing the geometry of slope landslides.
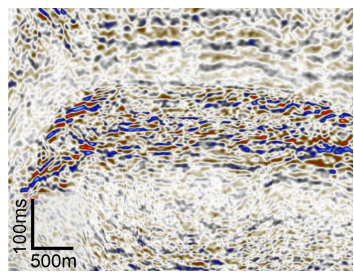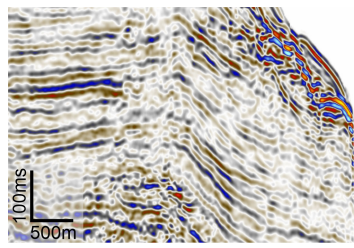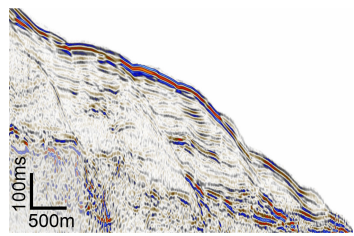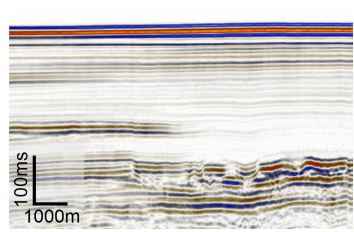
5 Discussion

5.1 Platform margin collapses initiating submarine canyons

Large-scale scalloped collapse is characterized by highly steep escarpments and spatially excavated by a serious of erosional morphologies such as canyons and channels, which has been revealed both in ancient and modern settings on the northeastern margin of the Zhongsha Platform (Figures 2, 4, 6, 7). This irregular convex-bankward embayment typically result from the destabilization of carbonate platform margins, which are associated with various factors. Key among these include rapid sedimentation rates, gravitational forces, oceanographic processes, tectonic activity, sea-level changes, tsunamis, storms, and earthquakes (Cook et al., 1972; Mullins et al., 1986; Mullins and Hine, 1989; George et al., 1995; Janson et al., 2010; Jo et al., 2015). For instance, catastrophic collapse has been revealed on the West Florida carbonate platform margin in the middle Miocene during a relative sea-level highstand. This event was attributed to rapid sediment accumulation, which led to

TABLE 3 Seismic facies description and interpretation.

|	Seismic facies	Description	Interpretation
1		Discontinuous, high amplitude, internal chaotic reflection, positive topographic relief, mound shape	Carbonate platform (Huang et al., 2020)
2		Simi-continuous, high amplitude, internal chaotic reflection, convex-up, vertical accretion	Reef (Huang et al., 2020)
3		Continuous, high amplitude, V- or U-shaped	Submarine canyon (Wu et al., 2022)
4		Horizontal, continuous, moderate to high amplitude	Gravity flows (Su et al., 2020)
5		Discontinuous, low to high amplitude, chaotic or semi-transparent reflection	Mass transport deposits (Qin et al., 2017)
6		Simi-continuous, low to high amplitude, wave shape	Cyclic steps (Wu et al., 2024)
7		Parallel, continuous, low to high amplitude	Pelagic deposits (Qin et al., 2017)
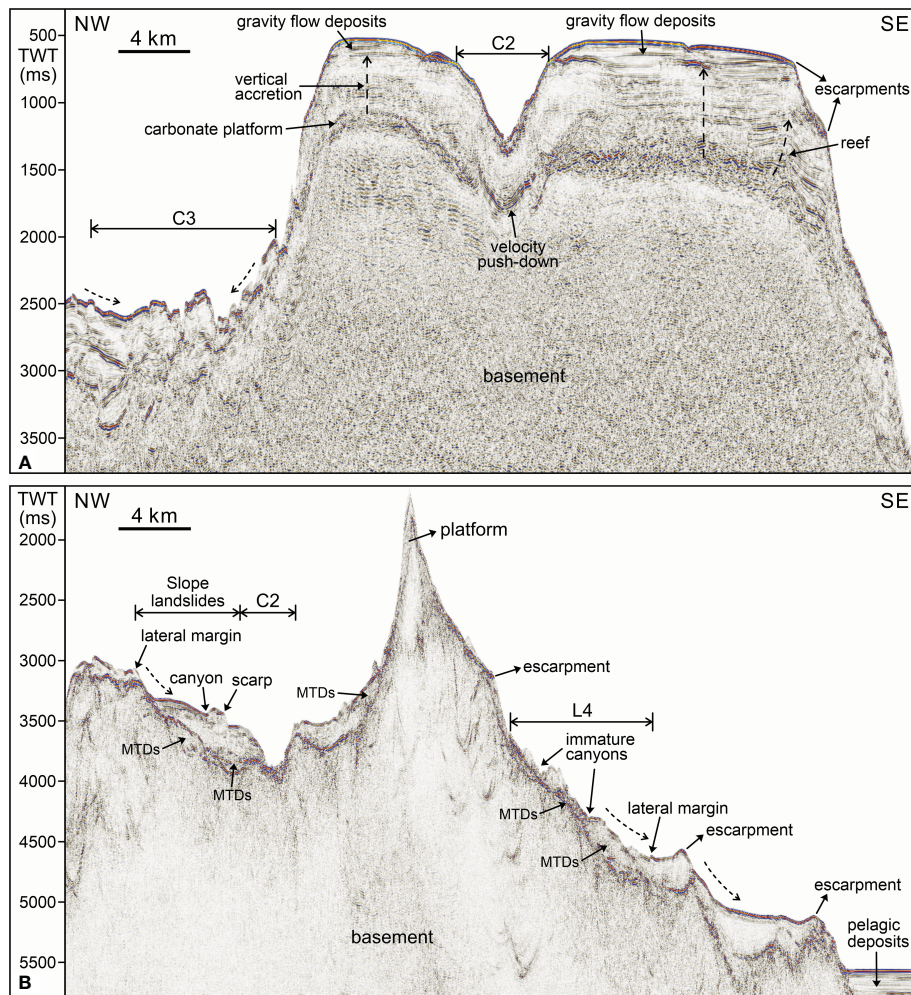
FIGURE 6
Two-dimensional seismic profiles crossing the northeast slope of the Zhongsha Platform. See locations in Figure 2A. **(A)** NW-SE oriented profile imaging the carbonate platform and upper slope. **(B)** NW-SE oriented profile imaging the middle to lower slope. MTDs: mass transport deposits.

gravitational instability and subsequent failure of the platform margin (Mullins et al., 1986). Similarly, George et al. (1995) documented a significant platform margin collapse during the Famennian in the Canning Basin, which was driven by rapid progradation and oversteepening of the reef margin. Additionally, sea-level fluctuations significantly influenced the platform margin collapses (George et al., 1995). Sea-level highstands contributed to higher carbonate production and efficient off-platform sediment transport, resulting in rapid sediment accumulation and highstand shedding along the platform margin (Grammer and Ginsburg, 1992; Schlager et al., 1994; Wilson and Roberts, 1995). Conversely, sea-level lowstands led to platform exposure, weathering, and karstification, further destabilizing the structural integrity (Bosellini et al., 1993; Spence and Tucker, 1997; Etienne et al., 2021). Numerical simulations of platform margin collapses demonstrated that sea-level changes alone were insufficient to induce collapses but can act as a predisposing factor, however, the synergistic effects of seismic shocks and active faulting played a significant role in triggering platform margin instability, which indicates that platform margin collapses are the result of the interaction of multiple factors

(Rusciadelli et al., 2003). Furthermore, the Lansdowne Bank is bordered by extensive margin collapses showing numerous slope bypass features (e.g. gullies, canyons, and channels). These catastrophic margin failures emphasize the significant impact of relative sea-level changes, retrogressive headward erosion, and tsunami waves (Etienne et al., 2021).

The Zhongsha Platform, affected by seasonally reversing monsoon, has gone through periods of sea-level highstands and lowstands, giving rise to the steep reef rims (Huang et al., 2020). The sediment grain size is relatively coarser on the platform top and progressively becomes finer downslope through mass movement and canyon processes (Figure 8). In this case study, the scalloped margin collapses of the Zhongsha Platform are attributed to reef aggradation/progradation and slope oversteepening resulting in gravitational instability, surface currents (e.g. tides, waves, and monsoon currents) leading to increased shear stress on the platform margin, and relative sea-level changes contributing to platform building outwards and density cascading. The mass wasting processes triggered by catastrophic failures result in extensive collapse and retreat of the outer platform margin, and
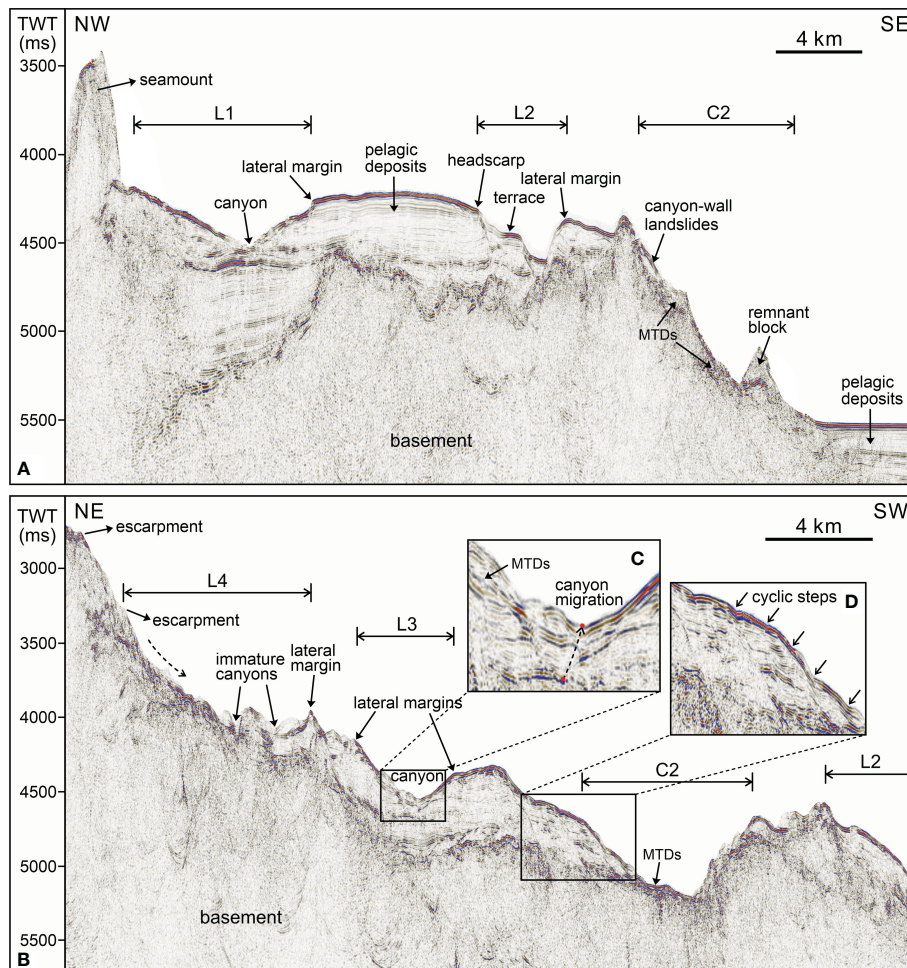
FIGURE 7
Two-dimensional seismic profiles crossing the northeast slope of the Zhongsha Platform. See locations in Figure 2A. **(A)** NW-SE oriented profile imaging the lower slope and oceanic basin. **(B)** NE-SW oriented profile imaging the middle to lower slope. **(C, D)** Zoom-in maps highlighting the inner seismic reflection structures.

subsequently cause a cascade of gravity flows that strongly incise and dissect the carbonate slopes capable of initiating submarine canyons. These canyons with headward erosion in turn to exacerbate the platform margin collapses. Tsunamis, tides, and waves occur frequently in the Zhongsha Platform, which is encircled by a deep oceanic basin (Figure 1). However, the specific effects of these external triggers remain unclear.

5.2 Slope landslides transforming to submarine canyons

Slope landslides are widely distributed and still exposed at the slope-toe adjacent to oceanic basin on the northeast Zhongsha Platform (Figures 2, 3). They are characterized by immature canyon morphologies with retrogressive headward erosion, notably L1, L3, and L4 (Figure 5). These slope landslides have the potential to evolve into mature canyons, backstepping from lower to upper slope and eventually connecting with platform margin. Such processes are indeed commonly implicated in the origin and evolution of slope

canyons in both carbonate and siliciclastic settings (Pratson and Coakley, 1996; Harris and Whiteway, 2011; Puga-Bernabéu et al., 2011; Mulder et al., 2012; Tournadour et al., 2017). In continental slopes, Wu et al. (2022) proposed an updated pattern for the formation and evolution of submarine canyons emphasizing the retrogressive failure mechanisms of mass transport deposits. This model involves three distinct phases, including initial failures with updip headscarps, retrogressively failed mass transport deposits, and the capture and convergence of canyons by pre-existing headscarps. In carbonate slopes, the canyon evolution models established on the northern slope of Little Bahama Bank and the Great Barrier Reef comprise three principal stages dominated by retrogressive erosion (Puga-Bernabéu et al., 2011; Tournadour et al., 2017): 1) slope destabilization initiating intra-slope failures, which can be trigger by sediment overpressure, fluid escapes, tectonics, earthquakes, and bottom currents (Principaud et al., 2015; Lüdmann et al., 2022); 2) successive retrogressive erosion resulting in the formation of canyon; 3) canyon headward erosion with headscarp failures reaching the upper slope and platform margin. The configuration of slope landslides observed in this study could be consistent with such pattern. L1, L3,
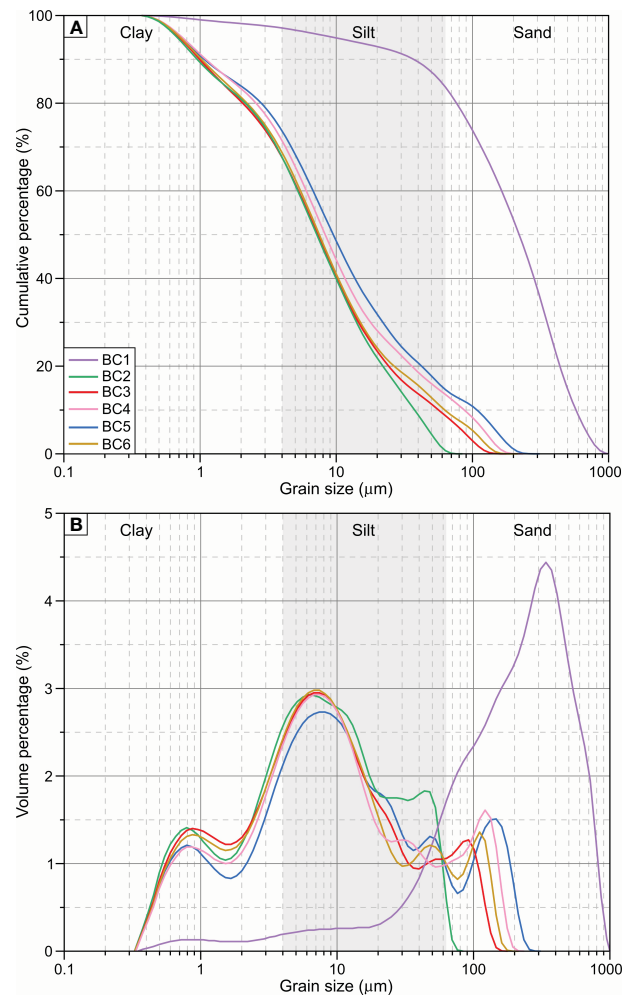
FIGURE 8
Cumulative **(A)** and frequency **(B)** curves showing the grain size distribution in surface sediments of the study area.

L4 and L5 are associated with the second stage, while L2 is more indicative of the first stage (Figure 5). The transition point from landslide to canyon in C2 is estimated to occur at a water depth of approximately 3420 m (Figures 4A, B). A series of knickpoints indicate retrogressive slope failures in the lower course of C2 (Figure 4A). The canyon-dominated zone extends for 35.8 km in length, whereas landslide-dominated zone spans a distance of 19 km (Figure 4B). Despite debris and blocks are not broadly present on the modern

seafloor, buried mass transport deposits are widely developed along the platform slopes (Figures 6, 7), indicating that landslides occurred prior to the erosional pathways. The deep cyclonic circulation that runs along the eastern slope of the Zhongsha Platform is highly susceptible to provoking slope destabilization and capable of carrying away landslide deposits and blocks.

5.3 Evolution model of submarine canyons

The morphology of C2 is distinguished by the erosion of numerous tributaries in the upper course, the transition of flow direction in the middle course, and the retrogressive slope landslides in the lower course (Figure 4). In light of the previous discussion, a four-stage conceptual model is proposed to elucidate the initiation of platform margin collapses and slope landslides, the inception of submarine canyons, and the interrelated evolution of these three elements in carbonate platform settings (Figure 9).

During inception stage (Figure 9A), off-platform sediment transport and associated processes delivered vast amounts of carbonate sediment from the inner platform to the outer platform

TABLE 4 Summary of the percentage content of grain size components in surface sediments.

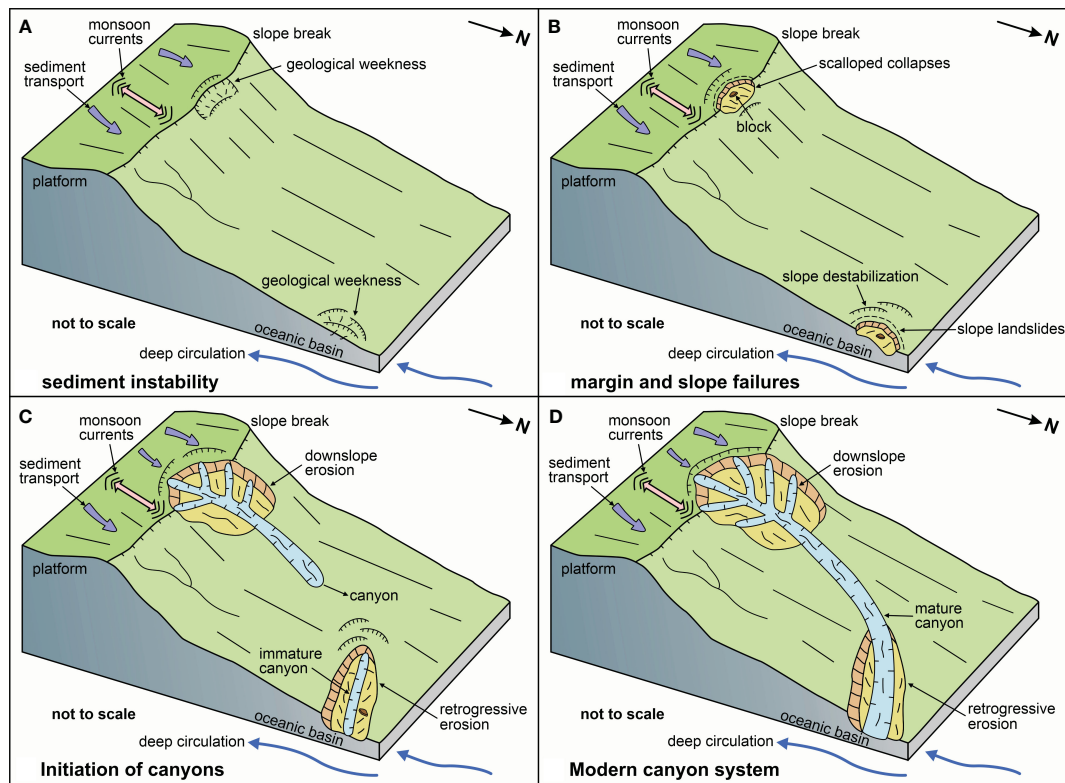| Core	Sand (%)	Silt (%)	Clay (%)
BC1	83.65	13.39	2.96
BC2	0.71	65.39	33.90
BC3	8.70	57.42	33.88
BC4	13.53	56.44	30.03
BC5	14.63	57.74	27.64
BC6	9.87	57.39	32.74

FIGURE 9
Conceptual model for the initiation and evolution of submarine canyons. **(A–D)** represent inception, expansion, development and present stages, respectively.

margin. Reef aggradation and sediment progradation lead to slope oversteepening, which in turn disrupts the stability of the original strata. During expansion stage (Figure 9B), oversteepened slope and gravitational instability resulted in sudden margin failures, forming large-scale scalloped collapses (Figures 2C, 4A). In addition, slope landslides were provoked by the disturbance of density cascading and deep currents in the lower slope (Figures 2C, 5). During development stage (Figure 9C), platform margin collapses and slope landslides have persistently developed in both horizontal and vertical scales, instigating sustained sediment gravity flows with the capacity to incise and shape submarine canyons. These mass wasting processes were exacerbated by tides, waves, density cascading, surface monsoon currents, and deep cyclonic circulation. The upper slope was characterized by downslope mass movement with dendritic canyon, while the lower slope was dominated by retrogressive erosion with headward escarpments and immature canyons (Figures 4, 5). At present stage (Figure 9D), sediment gravity flows progressed from the upper slope to the lower slope, veering northeastward into the structurally weak zone of the slope landslide area. The upper slope canyon scoured through slope landslide and eventually integrated with the lower slope canyon as it descended downslope, forming an elongated modern canyon that initially originated with a northeast direction and then transitioned to eastward orientation (Figure 4A).

5.4 Comparisons with other submarine canyons of carbonate platform

Carbonate platforms are dynamic marine environments characterized by the dominance of carbonate sediments derived from biological sources (Fauquembergue et al., 2023). Submarine canyons around carbonate platforms receive sediment inputs from both internal sources (carbonate debris, skeletal fragments) and external sources (terrestrial sediments, ocean currents) (Counts et al., 2018; Jorry et al., 2020). The Zhongsha Platform, situated in the central of SCS and distant from continental margin, has developed within a pure carbonate environment that is mainly composed of internal sources (Figure 1). In this study, submarine canyons in the northeast slope of the Zhongsha Platform are characterized by shelf-incised canyons exhibiting dendritic shape with numerous tributaries. They are triggered by platform margin collapses and incised by erosive gravity flows from upper slope to lower slope, which present different evolution processes compared to other submarine canyons in carbonate settings (Figure 9).

In the northern Little Bahama Bank, 18 slope-confined canyons are developed and strongly excavated along the carbonate slope. They are divided into upper linear part, middle widened part and lower mouth part, with water depths between 450 and 1000 m, an average length of 17 km, widths ranging from 5.5 to 20.4 km and a sinuosity of 1.03-1.21

(Mulder et al., 2012; Tournadour et al., 2017). In the western Great Bahama Bank, a series of regularly-spaced gullies incised the upper slope with water depths ranging from 250 to 600 m, an average length of 4 km and an average width of 750 m, resulting from density cascading processes (Principaud et al., 2015; Wunsch et al., 2017). Additionally, in the northern Great Barrier Reef, 19 submarine canyons are distinguished along the mixed carbonate-siliciclastic system including both shelf-incised and slope-confined canyons, with water depths between 30 and 2236 m, lengths ranging from 3.2 to 30.1 km and a sinuosity of 1-1.29. that include shelf-incised canyons and slope-confined canyons (Puga-Bernabéu et al., 2011). In these settings, the initiation and evolution of submarine canyons are resulted from slope destabilization and failure with retrogressive headward erosion from lower slope to upper slope (Puga-Bernabéu et al., 2011; Tournadour et al., 2017). However, spectacular large-scale margin collapses and slope failures have been identified along the entire outer reef rim in the Lansdowne Bank, which can generate submarine debris flows capable of souring erosive morphologies (Etienne et al., 2021). Submarine canyons around carbonate platforms present different geological processes, which can be attributed to sediment supply and oceanographic dynamics. Abundant sediment sources and high-energy hydrodynamic conditions contribute to slope oversteepening and lead to platform margin collapses.

6 Conclusion

1. Three submarine canyons are identified on the northeastern slope of the Zhongsha Platform. They are characterized by steep-sided V-shaped profiles in the upper course and U-shaped profiles in the lower course. C1 exhibit linear morphology terminating on the middle slope, while C2 and C3 present dendritic configuration extending towards the abyssal plain and oceanic basin.

2. A large-scale scalloped collapse has extensively eroded the northeastern margin and slope of the Zhongsha Platform. C2 originates from this margin failure in a northeastward orientation and subsequently converts to the eastward direction, with a water depth spanning from 651 to 4115 m, a length of 54.8 km and a sinuosity of 1.24. It is distinguished by numerous tributaries in the upper course and retrogressive slope landslides in the lower course.

3. Slope landslides extend from middle-lower slope towards oceanic basin trending in an eastward direction with a water depth ranging from 2300 to 4200 m and an area of 68-193 km^2. These landslides present an elongated shape in space and a concave profile in cross-section, characterized by numerous headscarps, lateral margins, inner scarps and immature canyons. A train of escarpments exhibit significant elevation relief at the landslide heads with retrogressive erosion.

4. Scalloped margin collapses are resulted from reef aggradation/progradation, slope oversteepening, surface monsoon currents, and relative sea-level changes. Slope landslides are triggered by the effects of slope destabilization, density cascading and deep cyclonic currents. These mass wasting processes can give rise to successive gravity flows capable of incising submarine canyons.

5. A four-stage conceptual model is proposed to illustrate the genesis and evolution of C2: Inception stage, sediment instability on platform margin and slope-toe; Expansion stage, the occurrence of platform margin collapses and slope landslides; Development stage, the exacerbation of failures and the inception of submarine canyons; Present stage, the configuration of modern canyon system.

6. Submarine canyons around carbonate platforms present distinct features that deserve attention due to their different triggering mechanisms and evolution processes. Platform margin collapses and slope landslides provide novel insights on sedimentary processes in isolated carbonate platform settings.

Data availability statement

The original contributions presented in the study are included in the article/supplementary material. Further inquiries can be directed to the corresponding authors.

Author contributions

JC: Validation, Writing – review & editing, Writing – original draft, Visualization, Software, Methodology, Investigation, Formal analysis, Data curation, Conceptualization. QL: Writing – review & editing, Validation, Resources, Project administration, Investigation, Funding acquisition. SW: Writing – review & editing, Validation, Resources, Project administration, Investigation, Funding acquisition. SL: Writing – review & editing, Resources, Project administration.

Funding

Acknowledgments

Conflict of interest

The authors declare that the research was conducted in the absence of any commercial or financial relationships that could be construed as a potential conflict of interest.

The author(s) declared that they were an editorial board member of Frontiers, at the time of submission. This had no impact on the peer review process and the final decision.

Publisher's note

References

Almeida, N. M. D., Vital, H., and Gomes, M. P. (2015). Morphology of submarine canyons along the continental margin of the Potiguar Basin, NE Brazil. *Mar. Pet. Geol.* 68, 307–324. doi: 10.1016/j.marpetgeo.2015.08.035

Betzler, C., Hübscher, C., Lindhorst, S., Reijmer, J. J. G., Römer, M., Droxler, A. W., et al. (2015). Monsoon-induced partial carbonate platform drowning (Maldives, Indian Ocean). *Geology* 37, 867–870. doi: 10.1130/G25702A.1

Betzler, C., Lindhorst, S., Eberli, G. P., Lüdmann, T., Möbius, J., Ludwig, J., et al. (2014). Periplatform drift: The combined result of contour current and off-bank transport along carbonate platforms. *Geology* 42, 871–874. doi: 10.1130/G35900.1

Betzler, C., Lindhorst, S., Lüdmann, T., Reijmer, J. J., Braga, J., Bialik, O. M., et al. (2021). Current and sea level control the demise of shallow carbonate production on a tropical bank (Saya de Malha Bank, Indian Ocean). *Geology* 49, 1431–1435. doi: 10.1130/G49090.1

Bosellini, A., Neri, C., and Luciani, V. (1993). Platform margin collapses and sequence stratigraphic organization of carbonate slopes: Cretaceous-Eocene, Gargano Promontory, southern Italy. *Terra Nova* 5, 282–297. doi: 10.1111/j.1365-3121.1993.tb00259.x

Chen, J., Wu, S., Li, Q., Wei, C., Fu, G., Chen, W., et al. (2024). Morphology and evolution of submarine canyons around the Zhongsha Platform, South China Sea: Implications for sedimentary processes in a modern isolated carbonate setting. *Mar. Geol.* In Press. 10. doi: 10.1016/j.margeo.2024.107362

Chen, J., Wu, S., Liu, S., Chen, W., Qin, Y., and Wan, X. (2022). Sedimentary Dynamics in the distal margin around isolated carbonate platforms of the northern South China Sea. *Front. Earth Sci.* 10. doi: 10.3389/feart.2022.884921

Cook, H. E., McDaniel, P. N., Mountjoy, E. W., and Pray, L. C. (1972). Allochthonous carbonate debris flows at Devonian bank ("reef") margins, Alberta, Canada. *Bull. Can. Petrol. Geol.* 20, 439–497. doi: 10.35767/gscpgbull.20.3.439

Counts, J. W., Jorry, S. J., Leroux, E., Miramontes, E., and Jouet, G. (2018). Sedimentation adjacent to atolls and volcano-cored carbonate platforms in the Mozambique Channel (SW Indian Ocean). *Mar. Geol.* 404, 41–59. doi: 10.1016/j.margeo.2018.07.003

Courgeon, S., Jorry, S. J., Camoin, G. F., BouDagher-Fadel, M. K., Jouet, G., Révillon, S., et al. (2016). Growth and demise of Cenozoic isolated carbonate platforms: New insights from the Mozambique Channel seamounts (SW Indian Ocean). *Mar. Geol.* 380, 90–105. doi: 10.1016/j.margeo.2016.07.006

Etienne, S., Roy., P. L., Tournadour, E., Roest, W. R., Jorry, S., Collot, J., et al. (2021). Large-scale margin collapses along a partly drowned, isolated carbonate platform (Lansdowne Bank, SW Pacific Ocean). *Mar. Geol.* 436, 106477. doi: 10.1016/j.margeo.2021.106477

Fang, G., Wang, G., Fang, Y., and Fang, W. (2012). A review on the South China Sea western boundary current. *Acta Oceanol. Sin.* 31, 1–10. doi: 10.1007/s13131-012-0231-y

Fauquembergue, K., Ducassou, E., Mulder, T., Reijmer, J. J. G., Borgomano, J., Recouvreur, A., et al. (2023). Quaternary sedimentary processes on the Bahamas: From platform to abyss. *Mar. Geol.* 459, 107044. doi: 10.1016/j.margeo.2023.107044

Franke, D., Savva, D., Pubellier, M., Steuer, S., Mouly, B., Auxietre, J. L., et al. (2014). The final rifting evolution in the South China Sea. *Mar. Pet. Geol.* 58, 704–720. doi: 10.1016/j.marpetgeo.2013.11.020

Gan, J., Kung, H., Cai, Z., Liu, Z., Hui, C., and Li, J. (2022). Hotspots of the stokes rotating circulation in a large marginal sea. *Nat. Commun.* 13, 2223. doi: 10.1038/s41467-022-29610-z

George, A. D., Playford, P. E., and Powell, C. M. (1995). Platform-margin collapse during Famennian reef evolution, Canning Basin, Western Australia. *Geology* 23, 691–694. doi: 10.1130/0091-7613(1995)023<0691:pmcdfr>2.3.co;2

Grammer, G. M., and Ginsburg, R. N. (1992). Highstand versus lowstand deposition on carbonate platform margins: insight from Quaternary foreslopes in the Bahamas. *Mar. Geol.* 103, 125–136. doi: 10.1016/0025-3227(92)90012-7

Haq, B. U., Hardenbol, J., and Vail, P. R. (1987). Chronology of fluctuating sea levels since the Triassic. *Science* 235, 1156–1167. doi: 10.1126/science.235.4793.1156

Harris, P. T., and Whiteway, T. (2011). Global distribution of large submarine canyons: Geomorphic differences between active and passive continental margins. *Mar. Geol.* 285, 69–86. doi: 10.1016/j.margeo.2011.05.008

Heijnen, M. S., Clare, M. A., Cartigny, M. J. B., Talling, P. J., Hage, S., Pope, E. L., et al. (2022). Fill, flush or shuffle: How is sediment carried through submarine channels to build lobes? *Earth Planet. Sci. Lett.* 584, 117481. doi: 10.1016/j.epsl.2022.117481

Huang, X., Betzler, C., Wu, S., Bernhardt, A., Eagles, G., Han, X., et al. (2020). First documentation of seismic stratigraphy and depositional signatures of Zhongsha atoll (Macclesfield Bank), South China Sea. *Mar. Pet. Geol.* 117, 104349. doi: 10.1016/j.marpetgeo.2020.104349

Janocko, M., Nemec, W., Henriksen, S., and Warcho, (2013). The diversity of deep-water sinuous channel belts and slope valley-fill complexes. *Mar. Pet. Geol.* 41, 7–34. doi: 10.1016/j.marpetgeo.2012.06.012

Janson, X., Eberli, G. P., Lomando, A. J., and Bonnaffé, F. (2010). "Seismic characterization of large-scale platform-margin collapse along the Zhujiang carbonate platform (Miocene) of the South China Sea, based on Miocene outcrop analogs from Mut Basin, Turkey," *Cenozoic Carbonate Systems of Australasia* (Tulsa, Oklahoma, U.S.A.: SEPM Society for Sedimentary Geology), 79–98.

Jo, A., Eberli, G. P., and Grasmueck, M. (2015). Margin collapse and slope failure along southwestern Great Bahama Bank. *Sedimentary Geology* 317, 43–52. doi: 10.1016/j.sedgeo.2014.09.004

Jorry, S. J., Camoin, G. F., Jouet, G., Roy, P. L., Vella, C., Courgeon, S., et al. (2016). Modern sediments and Pleistocene reefs from isolated carbonate platforms (Iles Eparses, SW Indian Ocean): A preliminary study. *Acta Oecologica* 72, 129–143. doi: 10.1016/j.actao.2015.10.014

Jorry, S. J., Jouet, G., Edinger, E. N., Toucanne, S., Counts, J. W., Miramontes, E., et al. (2020). From platform top to adjacent deep sea: New source-to-sink insights into carbonate sediment production and transfer in the SW Indian Ocean (Glorieuses archipelago). *Mar. Geol.* 423, 106144. doi: 10.1016/j.margeo.2020.106144

Koss, J. E., Ethridge, F. G., and Schumm, S. A. (1994). An experimental study of the effects of base-level change on fluvial, coastal plain and shelf systems. *Eur. J. Medicinal Chem.* 21, 65–69. doi: 10.1002/ddr.430070108

Lees, A. (1975). Possible influence of salinity and temperature on modern shelf carbonate sedimentation. *Mar. Geol.* 19, 159–198. doi: 10.1016/0025-3227(75)90067-5

Lemay, M., Grimaud, J. L., Cojan, I., Rivoirard, J., and Ors, F. (2020). Geomorphic variability of submarine channelized systems along continentalmargins: Comparison with fluvial meandering channels. *Mar. Pet. Geol.* 115, 104295. doi: 10.1016/j.marpetgeo.2020.104295

Li, J., Li, W., Alves, T. M., Rebesco, M., Wang, X., Li, S., et al. (2023). Controls on the morphology of closely spaced submarine canyons incising the continental slope of the northern South China Sea. *Geomorphology* 432, 108712. doi: 10.1016/j.geomorph.2023.108712

Li, Q., Wu, W., Liang, J., Kang, H., Liu, W., Wang, G., et al. (2020). Deep-water channels in the lower Congo basin: Evolution of the geomorphology and depositional environment during the Miocene. *Mar. Pet. Geol.* 115, 104260. doi: 10.1016/j.marpetgeo.2020.104260

Li, C., Xu, X., Lin, J., Sun, Z., Zhu, J., Yao, Y., et al. (2014). Ages and magnetic structures of the South China Sea constrained by deep tow magnetic surveys and IODP Expedition 349. *Geochem. Geophy. Geosy.* 15, 4958–4983. doi: 10.1002/2014GC005567

Liu, J. T., Hsu, R. T., Hung, J., Chang, Y., Wang, Y., Rendle-Bühring, R. H., et al. (2016). From the highest to the deepest: The Gaoping River–Gaoping Submarine Canyon dispersal system. *Earth-Science Rev.* 153, 274–300. doi: 10.1016/j.earscirev.2015.10.012

Lüdmann, T., Betzler, C., Lindhorst, S., Lahajnar, N., and Hübscher, C. (2022). Submarine landsliding in carbonate ooze along low-angle slopes (Inner Sea, Maldives). *Mar. Pet. Geol.* 136, 105403. doi: 10.1016/j.marpetgeo.2021.105403

Mayall, M., Jones, E., and Casey, M. (2006). Turbidite channel reservoirs e key elements in facies prediction and effective development. *Mar. Pet. Geol.* 23, 821e841. doi: 10.1016/j.marpetgeo.2006.08.001

McHargue, T., Pyrcz, M. J., Sullivan, M. D., Clark, J. D., Fildani, A., Romans, B. W., et al. (2011). Architecture of turbidite channel systems on the continental slope: Patterns and predictions. *Mar. Pet. Geol.* 28, 728–743. doi: 10.1016/j.marpetgeo.2010.07.008

Mountjoy, J. J., Howarth, J. D., Orpin, A. R., Barnes, P. M., Bowden, D. A., Rowden, A. A., et al. (2018). Earthquakes drive large-scale submarine canyon development and sediment supply to deep-ocean basins. *Sci. Adv.* 4, eaar3748. doi: 10.1126/sciadv.aar374

Mulder, T., Ducassou, E., Gillet, H., Hanquiez, V., Tournadour, E., Combes, J., et al. (2012). Canyon morphology on a modern carbonate slope of the Bahamas: Evidence of regional tectonic tilting. *Geology* 40, 771–774. doi: 10.1130/G33327.1

Mulder, T., Gillet, H., Hanquiez, V., Ducassou, E., Fauquembergue, K., Principaud, M., et al. (2017). Carbonate slope morphology revealing a giant submarine canyon (Little Bahama Bank, Bahamas). *Geology* 46, 31–34. doi: 10.1130/G39527.1

Mullins, H. T., Gardulski, A. F., and Hine, A. C. (1986). Catastrophic collapse of the west Florida carbonate platform margin. *Geology* 14, 167. doi: 10.1130/0091-7613 (1986) 14<167:CCOTWF>2.0.CO;2

Mullins, H. T., and Hine, A. C. (1989). Scalloped bank margins: Beginning of the end for carbonate platforms? *Geology* 17, 30. doi: 10.1130/0091-7613(1989)017<0030: SBMBOT<2.3.CO;2

Petrovic, A., Reijmer, J. J. G., Alsaihati, S. H. M., Nommensen, D., and Vahrenkamp, V. (2023). Sediment dynamics and geomorphology of a submarine carbonate platform canyon system situated in an arid climate setting. *Sedimentology*. 70, 2241–2271. doi: 10.1111/sed.13120

Pettinga, L. A., and Jobe, Z. R. (2020). How submarine channels (re)shape continental margins. *J. Sediment. Res.* 90, 1581–1600. doi: 10.2110/jsr.2020.72

Pomar, L. (2001). Types of carbonate platforms: a genetic approach. *Basin Res.* 13, 313–334. doi: 10.1046/j.0950-091x.2001.00152.x

Pomar, L., and Hallock, P. (2008). Carbonate factories: A conundrum in sedimentary geology. *Earth-Science Rev.* 87, 134–169. doi: 10.1016/j.earscirev.2007.12.002

Posamentier, H. W. (2003). Depositional elements associated with a basin floor channel-levee system: case study from the Gulf of Mexico. *Mar. Pet. Geol.* 20, 677–690. doi: 10.1016/j.marpetgeo.2003.01.002

Pratson, L. F., and Coakley, B. J. (1996). A model for the headward erosion of submarine canyons induced by downslope-eroding sediment flows. *GSA Bull.* 108, 225–234. doi: 10.1130/0016-7606(1996)108<0225:AMFTHE>2.3.CO;2

Principaud, M., Mulder, T., Gillet, H., and Borgomano, J. (2015). Large-scale carbonate submarine mass-wasting along the northwestern slope of the Great Bahama Bank (Bahamas): Morphology, architecture, and mechanisms. *Sed. Geol.* 317, 27–42. doi: 10.1016/j.sedgeo.2014.10.008

Principaud, M., Ponte, J., Mulder, T., Gillet, H., Robin, C., and Borgomano, J. (2017). Slope-to-basin stratigraphic evolution of the northwestern Great Bahama Bank (Bahamas) during the Neogene to Quaternary: interactions between downslope and bottom currents deposits. *Basin Res.* 29, 699–724. doi: 10.1111/bre.12195

Puga-Bernabéu, Á., Webster, J. M., Beaman, R. J., and Guilbaud, V. (2011). Morphology and controls on the evolution of a mixed carbonate–siliciclastic submarine canyon system, Great Barrier Reef margin, north-eastern Australia. *Mar. Geol.* 289, 100–116. doi: 10.1016/j.margeo.2011.09.013

Puga-Bernabéu, Á., Webster, J. M., Beaman, R. J., and Guilbaud, V. (2013). Variation in canyon morphology on the Great Barrier Reef margin, north-eastern Australia: The influence of slope and barrier reefs. *Geomorphology* 191, 35–50. doi: 10.1016/j.geomorph.2013.03.001

Qin, Y., Alves., T. M., Constantine., J., and Gamboa, D. (2017). The role of mass wasting in the progressive development of submarine channels (Espírito Santo Basin, SE Brazil). *J. Sediment. Res.* 87, 500–516. doi: 10.2110/jsr.2017.18

Qu, T., Girton, J. B., and Whitehead, J. A. (2006). Deepwater overflow through Luzon Strait. *J. Geophys. Res. Oceans* 111, C01002. doi: 10.1029/2005JC003139

Reijmer, J. J. G. (2021). Marine carbonate factories: review and update. *Sedimentology* 68, 1729–1796. doi: 10.1111/sed.12878

Reolid, J., Betzler, C., Braga, J. C., Lüdmann, T., Ling, A., and Eberli, G. P. (2020). Facies and geometry of drowning steps in a Miocene carbonate platform (Maldives). *Palaeogeography, Palaeoclimatology, Palaeoecology* 538, 109455. doi: 10.1016/j.palaeo.2019.109455

Ribeiro, R. F., Dominguez, J. M. L., Santos, A. A., and Rangel, A. G. A. N. (2021). Continuous canyon-river connection on a passive margin: The case of São Francisco Canyon (eastern Brazil). *Geomorphology* 375, 107549. doi: 10.1016/j.geomorph.2020.107549

Rusciadelli, G., Sciarra, N., and Mangifesta, M. (2003). 2D modelling of large-scale platform margin collapses along an ancient carbonate platform edge (Maiella Mt., Central Apennines, Italy): geological model and conceptual framework. *Palaeogeogr. Palaeocl.* 200, 245–262. doi: 10.1016/S0031-0182(03)00453-X

Saller, A., and Dharmasamadhi, I. N. W. (2012). Controls on the development of valleys, canyons, and unconfined channel-levee complexes on the Pleistocene Slope of East Kalimantan, Indonesia. *Mar. Pet. Geol.* 29, 15–34. doi: 10.1016/j.marpetgeo.2011.09.002

Schlager, W. (2005). *Carbonate sedimentology and sequence stratigraphy* (Tulsa, Oklahoma, U.S.A.: SEPM (Society for Sedimentary Geology), 200.

Schlager, W., Reijmer, J. J. G., and Droxler, A. W. (1994). Highstand shedding of carbonate platforms. *J. Sediment. Res.* 64, 270281. doi: 10.1306/D4267FAA-2B26-11D7-8648000102C1865D

Serra, S. C., Martínez-Loriente, S., Gràcia, E., Urgeles, R., Vizcaino, A., Perea, H., et al. (2020). Tectonic evolution, geomorphology and influence of bottom currents along a large submarine canyon system: The São Vicente Canyon (SW Iberian margin). *Mar. Geol.* 426, 106219. doi: 10.1016/j.margeo.2020.106219

Shen, X., Hu, B., Yan, H., Dodson, J., Zhao, J., Li, J., et al. (2022). Reconstruction of Kuroshio intrusion into the South China Sea over the last 40 kyr. *Quarter. Sci. Rev.* 290, 107622. doi: 10.1016/j.quascirev.2022.107622

Shepard, F. P. (1972). Submarine canyons. *Earth-Science Rev.* 8, 1–12. doi: 10.1016/ 0012-8252(72)90032-3

Spence, G. H., and Tucker, M. E. (1997). Genesis of limestone megabreccias and their significance in carbonate sequence stratigraphic models: a review. *Sedimentary Geology* 112, 163–193. doi: 10.1016/S0037-0738(97)00036-5

Su, M., Lin, Z., Wang, C., Kuang, Z., Liang, J., Chen, H., et al. (2020). Geomorphologic and infilling characteristics of the slope-confined submarine

canyons in the Pearl River Mouth Basin, northern South China Sea. *Mar. Geol.* 424, 106166. doi: 10.1016/j.margeo.2020.106166

Sun, Y., Wang, D., Canals, A., Alves, T. M., Wang, W., Zhu, Y., et al. (2023). Bedform evolution along a submarine canyon in the South China Sea: New insights from an autonomous underwater vehicle survey. *Sedimentology* 71, 793–826. doi: 10.1111/sed.13152

Taylor, B., and Hayes, D. E. (1983). Origin and history of the South China Sea Basin. *Geophysical Monograph Ser.* 27, 23–56. doi: 10.1029/gm027p0023

Tournadour, E., Mulder, T., Borgomano, J., Gillet, H., Chabaud, L., Ducassou, E., et al. (2017). Submarine canyon morphologies and evolution in modern carbonate settings: The northern slope of Little Bahama Bank, Bahamas. *Mar. Geol.* 391, 76–97. doi: 10.1016/j.margeo.2017.07.014

Tubau, X., Paull, C. K., Lastras, G., Caress, D. W., Canals, M., Lundsten, E., et al. (2015). Submarine canyons of Santa Monica Bay, Southern California: Variability in morphology and sedimentary processes. *Mar. Geol.* 365, 61–79. doi: 10.1016/j.margeo.2015.04.004

Wang, A., Du, Y., Peng, S., Liu, K., and Huang, R. X. (2018). Deep water characteristics and circulation in the South China Sea. *Deep Sea Res. Part I* 134, 55–63. doi: 10.1016/j.dsr.2018.02.003

Wang, B., Zhong, G., Wang, L., He, M., Zhu, B., Guo, Y., et al. (2023). Morphology, seismic stratigraphy, and tectonic control of the Yitong submarine canyons – fan apron system in the Northern South China Sea. *Mar. Petrol. Geol.* 155, 106347. doi: 10.1016/ j.marpetgeo.2023.106347

Warnke, F., Schwenk, T., Miramontes, E., Spiess, V., Wenau, S., Bozzano, G., et al. (2023). Evolution of complex giant seafloor depressions at the northern Argentine continental margin (SW Atlantic Ocean) under the influence of a dynamic bottom current regime. *Front. Earth Sci.* 11. doi: 10.3389/feart.2023.1117013

Wentworth, C. K. (1922). A scale of grade and class terms for clastic sediments. *J. Geology.* 30, 377–392. doi: 10.1086/622910

Wilson, P. A., and Roberts, H. H. (1992). Carbonate-periplatform sedimentation by density flows: a mechanism for rapid off-bank and vertical transport of shallow-water fines. *Geology* 20, 713–716. doi: 10.1130/0091-7613(1993)0212.3.co;2

Wilson, P. A., and Roberts, H. H. (1995). Density cascading: off-shelf sediment transport, evidence and implications, Bahama Banks. *J. Sediment. Res.* 65, 45–56. doi: 10.1306/D426801D-2B26-11D7-8648000102C1865D

Wu, N., Nugraha, H. D., Zhong, G., and Steventon, M. J. (2022). The role of mass-transport complexes in the initiation and evolution of submarine canyons. *Sedimentology* 69, 2181–2202. doi: 10.1111/sed.12987

Wu, S., Yang, Z., Wang, D., Lü, F., Lüdmann, T., Fulthorpe, C., et al. (2014). Architecture, development and geological control of the Xisha carbonate platforms, northwestern South China Sea. *Mar. Geol.* 350, 71–83. doi: 10.1016/ j.margeo.2013.12.016

Wu, S., Zhang, X., Yang, Z., Wu, T., Gao, J., and Wang, D. (2016). Spatial and temporal evolution of Cenozoic carbonate platforms on the continental margins of the South China Sea: Response to opening of the ocean basin. *Interpretation* 4, SP1–SP19. doi: 10.1190/INT-2015-0162.1

Wu, N., Zhong, G., Niyazi, Y., Wang, B., Nugraha, H. D., and Steventon, M. J. (2024). Transformation of dense shelf water cascade into turbidity currents: Insights from high-resolution geophysical datasets. *Earth Planetary Sci. Lett.* 626, 118547. doi: 10.1016/j.epsl.2023.118547

Wunsch, M., Betzler, C., Eberli, G. P., Lindhorst, S., Lüdmann, T., and Reijmer, J. J. G. (2018). Sedimentary dynamics and high-frequency sequence stratigraphy of the southwestern slope of Great Bahama Bank. *Sed. Geol.* 363, 96–117. doi: 10.1016/ j.sedgeo.2017.10.013

Wunsch, M., Betzler, C., Lindhorst, S., Lüdmann, T., and Eberli, G. P. (2017). Sedimentary dynamics along carbonate slopes (Bahamas archipelago). *Sedimentology* 64, 631–657. doi: 10.1111/sed.12317

Xu, Q., Zhang, L., Xiao, X., Zhou, C., Wang, F., and Hu, D. (2023). Seasonal link between deepwater overflow through the Luzon strait and deep Western boundary current in the Philippine Sea. *Geophys. Res. Lett.* 50, e2023GL105405. doi: 10.1029/2023GL105405

Yang, H., Liu, Q., Liu, Z., Wang, D., and Liu, X. (2002). A general circulation model study of the dynamics of the upper ocean circulation of the South China Sea. *J. Geophys. Res. Oceans* 107, 3085. doi: 10.1029/2001JC001084

Yang, Q., Zhao, W., Liang, X., and Tian, J. (2016). Three-dimensional distribution of turbulent mixing in the South China Sea. *J. Phys. Oceanogr.* 46, 769–788. doi: 10.1175/ JPO-D-14-0220.1

Yao, Y., Liu, H., Yang, C., Han, B., Tian, J., Yin, Z., et al. (2012). Characteristics and evolution of Cenozoic sediments in the Liyue Basin, SE South China Sea. *J. Asian Earth Sci.* 60, 114–129. doi: 10.1016/j.jseaes.2012.08.003

Yu, K., Miramontes, E., Alves, T. M., Li, W., Liang, L., Li, S., et al. (2021). Incision of submarine channels over pockmark trains in the South China Sea. *Geophys. Res. Lett.* 48, e2021GL092861. doi: 10.1029/2021GL092861

Zhong, G., and Peng, X. (2021). Transport and accumulation of plastic litter in submarine canyons—The role of gravity flows. *Geology* 49, 581–586. doi: 10.1130/ G48536.1

Zhu, Y., Sun, J., Wang, Y., Li, S., Xu, T., Wei, Z., et al. (2019). Overview of the multi-layer circulation in the South China Sea. *Prog. Oceanogr.* 175, 171–182. doi: 10.1016/ j.pocean.2019.04.001